Three-body model of light nuclei with microscopic nonlocal interactions

M. Theeten,[1,2] H. Matsumura,[3,*] M. Orabi,[3] D. Baye,[1,2] P. Descouvemont,[2] Y. Fujiwara,[4] and Y. Suzuki[5]
[1]*Physique Quantique, C. P. 165/82, Université Libre de Bruxelles (ULB), B-1050 Brussels, Belgium*
[2]*Physique Nucléaire Théorique et Physique Mathématique, C. P. 229, Université Libre de Bruxelles (ULB), B-1050 Brussels, Belgium*
[3]*Graduate School of Science and Technology, Niigata University, Niigata 950-2181, Japan*
[4]*Department of Physics, Kyoto University, Kyoto 606-8502, Japan*
[5]*Department of Physics, and Graduate School of Science and Technology, Niigata University, Niigata 950-2181, Japan*
(Received 30 August 2007; published 27 November 2007)

A three-body cluster model involving microscopic nonlocal interactions is developed and compared with a fully microscopic cluster model. The energy-independent nonlocal interactions are obtained from a renormalization of the energy-dependent kernels of the resonating-group method. Such interactions are derived for the $\alpha\alpha$ and αn systems. The role and importance of nonlocality are discussed. These interactions are employed in three-body studies of the αnn, $\alpha\alpha n$, and 3α descriptions of the ^{6}He, ^{9}Be, and ^{12}C nuclei. A comparison with fully microscopic calculations provides a measure of the importance of three-cluster exchanges in those states. The differences between both cluster-model calculations are in general small, except in the densities at short distances.

DOI: 10.1103/PhysRevC.76.054003 PACS number(s): 21.60.Gx, 21.45.+v, 27.20.+n

I. INTRODUCTION

The microscopic cluster model provides a consistent description of the spectroscopy and reactions of light nuclei [1–3]. In this model, the nucleons are grouped into substructures known as clusters. The merit of this microscopic model is that it starts from two-nucleon potentials and takes an exact account of antisymmetrization and of good quantum numbers. Its main limitations are the use of effective forces and simplified descriptions of the internal structure of the clusters. In spite of the progresses of *ab initio* calculations [4], the microscopic cluster model remains very useful because it provides tractable wave functions both for bound and continuum states that can be employed in various reaction and decay studies. Of course, the cluster approximation makes it necessary to use effective nucleon-nucleon interactions.

Some nuclei display a three-cluster structure such as ^{9}Be or the halo nucleus ^{6}He. Other such as ^{12}C clearly display this structure in some excited states but its presence in the ground state has raised questions. Nevertheless the microscopic cluster model is able to reproduce the main properties of the ^{6}He, ^{9}Be, and ^{12}C nuclei without adjustable parameters except for the choice of the effective nucleon-nucleon interaction.

The description of three-cluster systems by fully microscopic calculations can however be very heavy and require large amounts of computer time. Simpler three-cluster models involving phenomenological local cluster-cluster interactions are therefore often used to analyze their decays and reactions.

These phenomenological cluster models are however less well established and sometimes controversial. The ^{12}C case is a typical example. The microscopic cluster model provides a satisfactory qualitative description of several states of ^{12}C [5–7]. Macroscopic 3α models based on phenomenological local $\alpha\alpha$ interactions, though physically appealing, fail to reproduce even qualitatively the properties of the ^{12}C ground state [8–11]. Any local potential which reproduces the $\alpha\alpha$ phase shifts yields very poor results, in disagreement with experiment and with microscopic models.

That the $\alpha\alpha$ potential can not be local for describing ^{12}C is not surprising. The interaction between composite particles is intrinsically nonlocal because of the exchange symmetry of identical constituents. Such interactions between two clusters can be derived microscopically from effective nucleon-nucleon forces within the resonating-group method (RGM) [1–3]. A first attempt to use energy-dependent nonlocal $\alpha\alpha$ RGM kernels has been developed in Refs. [12,13] in a study of ^{12}C. The energy dependence of the $\alpha\alpha$ nonlocal interaction raises a difficulty. This energy is well defined in a two-body system but not in a three-body system. Using some average energy provides fair results for ^{12}C [14] but not for other three-cluster systems [15]. Hence the energy dependence must be eliminated from the RGM equation. The principle of this elimination is known for a long time [2,16–18]. Recently, we have shown that this procedure leads to a consistent description of the 0^+ states of ^{12}C case, in semiquantitative agreement with fully microscopic calculations [19].

The purpose of the present study is to pursue the analysis of the three-body model with energy-independent RGM forces. To this end, we extend the model to ^{9}Be (as $\alpha\alpha n$) and ^{6}He (as αnn) in order to improve our understanding of the importance of nonlocality which is based until now on the sole ^{12}C case. This model is called semimicroscopic hereafter. We consider several effective nucleon-nucleon forces. We also analyze the nonlocality of the $\alpha\alpha$ and αn forces and try to derive simpler approximations.

In Sec. II, we summarize the two-cluster RGM theory and the derivation of the renormalized RGM potential. In Sec. III, we discuss the role and importance of nonlocality and propose an approximation. The semimicroscopic and microscopic three-cluster models are described in Sec. IV. In

[*]Present address: Mizuho Information & Research Institute Inc., Chiyoda-ku, Tokyo 100-8210, Japan

Sec. V, semimicroscopic and microscopic results are presented and compared for the ^{12}C, ^{9}Be, and ^{6}He nuclei. Section VI is devoted to concluding remarks.

II. RENORMALIZED RGM FOR TWO-CLUSTER SYSTEMS

A. RGM equation

The RGM wave function of the two-cluster $(A+B)$ system with the relative motion function χ is expressed as

$$\Psi = \mathcal{A}\phi_A\phi_B\chi(\boldsymbol{x}) = \int \chi(\boldsymbol{r})\Phi(\boldsymbol{r})d\boldsymbol{r}, \tag{1}$$

with the basis function

$$\Phi(\boldsymbol{r}) = \mathcal{A}\phi_A\phi_B\delta(\boldsymbol{x}-\boldsymbol{r}), \tag{2}$$

where ϕ_A and ϕ_B are the cluster internal wave functions and $\mathcal{A}$ is an antisymmetrizer. Here $\boldsymbol{x}$ is the relative coordinate between the clusters, while $\boldsymbol{r}$ is a parameter or generator coordinate corresponding to $\boldsymbol{x}$. The cluster internal wave functions ϕ_A and ϕ_B are assumed to be described with harmonic-oscillator (HO) functions with a common size parameter.

The RGM equation for χ reads [1–3]

$$(T+V+\varepsilon K)\chi = \varepsilon\chi, \tag{3}$$

with

$$V = V_D + V^{EX}. \tag{4}$$

Here T is the intercluster kinetic energy, V_D is a local term called the direct potential, and the nonlocal potential V^{EX} comprises the exchange nonlocal kernels for the kinetic and potential energies (including the Coulomb term). The energy dependence arises from exchange effects in the overlap between basis functions. Indeed, the norm kernel can be written as

$$\mathcal{N}(\boldsymbol{r},\boldsymbol{r}') = \langle\Phi(\boldsymbol{r})|\Phi(\boldsymbol{r}')\rangle = \delta(\boldsymbol{r}-\boldsymbol{r}') - K(\boldsymbol{r},\boldsymbol{r}'). \tag{5}$$

The energy ε is defined with respect to the $A+B$ threshold.

By introducing a renormalized relative motion function

$$g = \sqrt{\mathcal{N}}\chi, \tag{6}$$

Eq. (3) can be converted into an equation involving an energy-independent potential

$$(T+V^{\mathrm{RGM}})g = \varepsilon g. \tag{7}$$

The nonlocal potential reads

$$V^{\mathrm{RGM}} = \mathcal{N}^{-1/2}(T+V)\mathcal{N}^{-1/2} - T = V + W. \tag{8}$$

Operator $\mathcal{N}^{-1/2}$ is defined over the Pauli allowed space (see Sec. II B). The additional operator W is the difference between the renormalized RGM potential V^{RGM} and the bare RGM potential V of Eq. (4),

$$W = \mathcal{N}^{-1/2}(T+V)\mathcal{N}^{-1/2} - (T+V). \tag{9}$$

It involves thus contributions from both the kinetic and potential energies.

In practice, the RGM equation must be projected on the total angular momentum of the system. In the following, we do not show the cluster spins and only display the dependence on the orbital angular momentum ℓ. In our calculations, however, all angular momenta and their couplings are taken into account.

B. Pauli forbidden states

For partial wave ℓ, a particular function $\chi_{f\ell}$ is called a Pauli forbidden states (PFS) if it satisfies the equation

$$\mathcal{N}_\ell\chi_{f\ell} = 0, \tag{10}$$

i.e.,

$$K_\ell\chi_{f\ell} = \chi_{f\ell}. \tag{11}$$

By using Eq. (3), this leads to

$$(T_\ell + V_\ell)\chi_{f\ell} = 0. \tag{12}$$

The eigenvalue problem

$$K_\ell\psi_{n\ell m} = \kappa_{n\ell}\psi_{n\ell m} \tag{13}$$

can be solved analytically. The eigenfunctions are HO functions $\psi_{n\ell m}$ [20]. The PFS are nothing but eigenfunctions of K_ℓ with eigenvalue $\kappa_{n\ell} = 1$. Operator $\mathcal{N}^{-1/2}$ in Eq. (9) is defined on the Pauli allowed space as

$$\mathcal{N}_\ell^{-1/2} = {\sum_n}'(1-\kappa_{n\ell})^{-1/2}P_{n\ell}, \tag{14}$$

where $P_{n\ell}$ is the projector on the HO subspace corresponding to n and ℓ and where the prime indicates that the PFS are excluded from the sum. By using Eqs. (9) and (12), this leads to

$$W_\ell\chi_{f\ell} = 0. \tag{15}$$

The PFS are thus trivial solutions of the RGM equation

$$\left(T_\ell + V_\ell^{\mathrm{RGM}}\right)\chi_{f\ell} = 0. \tag{16}$$

A solution g_ℓ of Eq. (7) is orthogonal to the PFS when $\varepsilon \neq 0$.

Two simple cases for the solution of Eq. (13) needed in the present study are

$$\kappa_{n\ell} = (-1/4)^{2n+\ell} \tag{17}$$

for $\alpha + N$, and

$$\kappa_{n\ell} = 4(1/2)^{2n+\ell} - 3\delta_{2n+\ell,0} \tag{18}$$

with ℓ even for $\alpha+\alpha$. Therefore only one PFS, ψ_{000}, exists for $\alpha+N$. For $\alpha+\alpha$, states with $\ell =$ odd are all PFS. For ℓ even, Eq. (18) provides three PFS, ψ_{000}, ψ_{100}, and ψ_{02m}.

C. Nonlocal potential W

With Eq. (14), the nonlocal kernel W_ℓ can be expressed as [19]

$$W_\ell(r,r') = rr'{\sum_{nn'}}'W_{nn'\ell}R_{n\ell}(r)R_{n'\ell}(r'), \tag{19}$$

where $R_{n\ell}(r)$ is the radial part of $\psi_{n\ell m}$. The coefficients $W_{nn'\ell}$ are given by

$$W_{nn'\ell} = \left[\frac{1}{\sqrt{(1-\kappa_{n\ell})(1-\kappa_{n'\ell})}} - 1\right]\langle\psi_{n\ell m}|T+V|\psi_{n'\ell m}\rangle. \tag{20}$$

Here V is assumed to be rotation-invariant, which makes its matrix elements independent of m. Use can be made of a recursion formula to calculate the HO functions with large n values.

Equations (19) and (20) indicate that the calculation of the matrix elements $\langle\psi_{n\ell m}|T+V|\psi_{n'\ell m}\rangle$ is needed to obtain the kernel W_ℓ. This calculation is facilitated by the use of the generating function of the HO wave functions, as shown in Appendix A.

The nonlocality pattern is very different between V_ℓ^{EX} and W_ℓ, as shown for $\alpha+\alpha$ in Ref. [19]. The potentials for $\ell=0$ and 2 show a rapidly oscillating behavior, which is related to the existence of the PFS. The absolute value of W_ℓ is smaller than that of V_ℓ^{EX} by about one order of magnitude.

III. INTERPRETATION AND APPROXIMATIONS

A. Potential function

A local potential is useful to give an intuitive picture for the potential between the clusters. Though there are some sophisticated techniques to make local a nonlocal potential, we here adopt one of the simplest methods used in Ref. [16] which introduces a potential function. The function is not a phase-equivalent potential to the original nonlocal potential, and our purpose is just to look at its different components. The potential function is defined by

$$\begin{aligned} U_\ell^{\mathrm{RGM}}(r) &= \int_{-2r}^{2r} V_\ell^{\mathrm{RGM}}\left(r+\frac{s}{2}, r-\frac{s}{2}\right) ds \\ &= V_D(r) + U_\ell^{NL}(r), \end{aligned} \tag{21}$$

which has a form similar to the Wigner transform at zero momentum. Equations (4) and (8) show that the nonlocality of the renormalized potential shows up in two terms: One is the V^{EX} term which originates from the RGM kernels, and the other is the W term which comes from the elimination of the energy-dependence. The potential function U_ℓ^{RGM} serves as a measure of the extent to which the antisymmetrization and the removal of the energy dependence modify V_D.

Figure 1 displays the potential function U_ℓ^{RGM} for the $\alpha\alpha$ system. The curves representing U_ℓ^{RGM} oscillate around V_D and their amplitude is significant even near the tail. The S, D, and I phase shifts calculated with the potential functions are in reasonable agreement with the RGM phase shifts, but the G phase shift deviates from the latter. The contributions of the kinetic, nuclear and Coulomb terms to the $U_\ell^{NL}(r)$ potentials are displayed in Fig. 2. The major contributor to U_ℓ^{NL} is the kinetic energy term, and its contribution is reduced by the nuclear potential energy term.

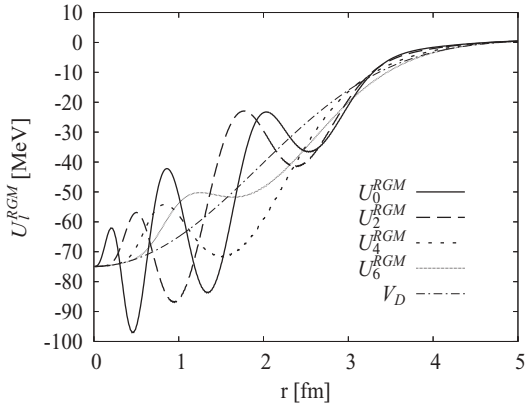

FIG. 1. The potential function $U_\ell^{\mathrm{RGM}}(r)$ and the direct potential V_D for the $\alpha\alpha$ system (the MN interaction is used).

B. Approximation of W

Though the evaluation of $W(\boldsymbol{r},\boldsymbol{r}')$ or $W_\ell(r,r')$ can be performed in the HO expansion as shown in Sec. II C, it may be useful to calculate $W(\boldsymbol{r},\boldsymbol{r}')$ approximately but more simply without using the expansion. We consider this possibility by expanding $\mathcal{N}^{-1/2}=(1-K)^{-1/2}$ in powers of K. It is possible to obtain the following series:

$$W = \sum_{i=1}^{\infty} W^{(i)}, \tag{22}$$

where

$$W^{(i)} = \sum_{j=0}^{i} \frac{(2j-1)!!\,(2i-2j-1)!!}{2^i\, j!(i-j)!} K^{i-j}(T+V)K^j. \tag{23}$$

In particular the first term is given by

$$W^{(1)} = \tfrac{1}{2}[K(T+V)+(T+V)K]. \tag{24}$$

When testing the convergence of expansion (22), we find that for a given ℓ all $W_\ell^{(i)}(r,r')$ have a shape similar to each other and that the ratio $W_\ell^{(i)}/W_\ell^{(i-1)}$ is about 1/4 for the $\alpha\alpha$ case. Thus the W potential can fairly well be approximated by $\lambda W^{(1)}$ with a suitable constant λ. We find that the quadratic difference between dense samplings of $\lambda W_\ell^{(1)}$ and W_ℓ displays a minimum around $\lambda\approx 1.30$ for $\alpha+\alpha$ and $\lambda\approx 1.05$ for $\alpha+N$. The approximation is better in the $\alpha+N$ case than in the $\alpha+\alpha$ case. We will test these approximations by replacing W with the simpler nonlocal term $\lambda W^{(1)}$ in V^{RGM} in the different three-body systems.

IV. SEMIMICROSCOPIC AND MICROSCOPIC THREE-CLUSTER MODELS

The calculations have been performed with various numerical techniques. Most results are checked in two completely independent calculations.

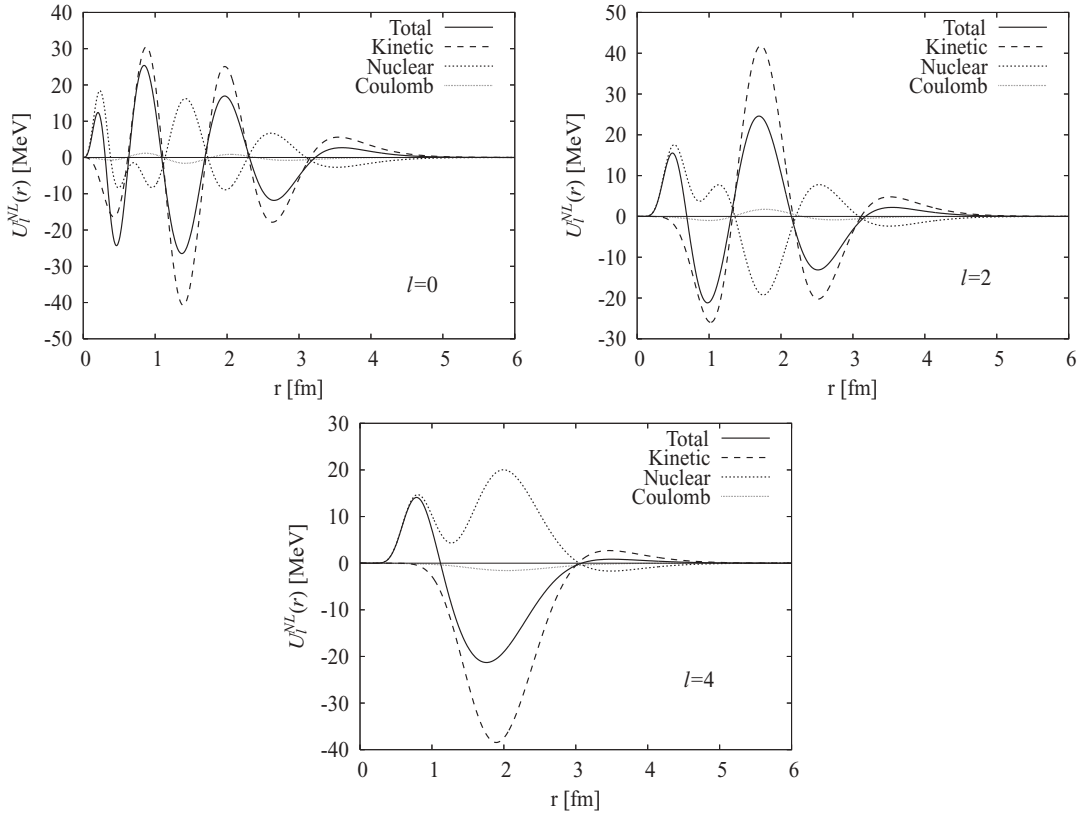

FIG. 2. Decomposition of the $\alpha\alpha$ $U_\ell^{NL}(r)$ potential into the kinetic energy, the nuclear potential and the Coulomb potential contributions (the MN interaction is used).

A. Semimicroscopic models

We describe two techniques of resolution of a three-body problem with nonlocal forces. The Hamiltonian of the system is given by

$$H = T_1 + T_2 + T_3 - T_{\text{c.m.}} + V_{12} + V_{13} + V_{23}, \qquad (25)$$

where T_i is the kinetic energy of cluster i, $T_{\text{c.m.}}$ is the kinetic energy of the center of mass, and V_{ij} a nucleus-nucleus interaction which, in the present case may be nonlocal.

In the hyperspherical-harmonics approach, calculations are performed in configuration space [23,24]. The wave function with quantum numbers $JM\pi$ is expanded as a function of standard hyperspherical harmonics $\mathcal{Y}_{\gamma K}^{JM}(\Omega_5)$ depending on five variables represented as Ω_5, i.e., the angular part of the Jacobi coordinates and the hyperangle which measures the ratio of these coordinates,

$$\Psi^{JM\pi}(\rho, \Omega_5) = \rho^{-5/2} \sum_{\gamma K} \chi_{\gamma K}^{J\pi}(\rho)\, \mathcal{Y}_{\gamma K}^{JM}(\Omega_5). \qquad (26)$$

Index K is the hypermomentum and index γ stands for different orbital momenta and spins. The functions $\chi_{\gamma K}^{J\pi}$ of the hyperradius ρ are solutions of a system of coupled equations. They are expanded in Lagrange functions [25] as

$$\chi_{\gamma K}^{J\pi}(\rho) = \sum_{i=1}^{N} c_{\gamma K i}^{J\pi} f_i(\rho). \qquad (27)$$

With a Lagrange basis, the calculation of matrix elements is simplified by an approximation based on a consistent Gauss quadrature. For example, matrix elements of a local function $v(\rho)$ become

$$\langle f_i(\rho)|v(\rho)|f_j(\rho)\rangle \approx v(\rho_i)\delta_{ij}, \qquad (28)$$

where ρ_i is a mesh point associated with Lagrange function f_i. Thanks to this approximation, the integration over ρ in the potential matrix elements only requires values of the (local or nonlocal) potentials at mesh points associated with the basis. Hence the Coulomb potential does not cause any difficulty. Energies of the three-body system are eigenvalues of a large matrix. The corresponding eigenvectors provide analytical approximations of the wave functions. Strikingly, the use of a Gauss quadrature does not reduce significantly the accuracy with respect to a variational calculation using the same basis, i.e., energies obtained with the exact left-hand side of Eq. (28) are very close to those obtained with the approximate right-hand side [23]. The elimination of PFS is explained in Ref. [24].

To provide a meaningful comparison with the microscopic model, we redefine the total wave function of the system as

$$\widetilde{\Psi}^{JM\pi} = \phi_1\phi_2\phi_3\Psi^{JM\pi}(\rho, \Omega_5), \qquad (29)$$

where ϕ_i is the translation-invariant internal wave function of cluster i. This new definition allows us to calculate observables where internal properties contribute, such as rms matter radii,

or form factors. It is also consistent with the microscopic definition of these observables.

In the Faddeev method, the calculations are performed in the momentum representation [12,13]. The nonlocality of the original two-body interaction has no obstacles, since the T-matrix used in the Faddeev calculation is nonlocal anyway. On the other hand, the Coulomb force can be treated only in an approximate way, by introducing a cut-off radius R_C (say $R_C = 10$ fm) that should be large enough to avoid the influence of the nuclear interaction. For three-cluster systems, it is essential to deal appropriately with the possible existence of PFS between two clusters. This can be achieved by using a new type of two-body T-matrix, $\widetilde{T}(\omega)$ or $\widetilde{T}(\omega, \varepsilon)$ [12], which satisfies some kind of orthogonality conditions

$$\begin{aligned} \langle \chi_f | [1 + G_0^{(+)}(\omega)\, \widetilde{T}(\omega, \varepsilon)] = 0, \\ [1 + \widetilde{T}(\omega, \varepsilon)\, G_0^{(+)}(\omega)] | \chi_f \rangle = 0. \end{aligned} \tag{30}$$

Here, $G_0^{(+)}(\omega)$ is the free Green function with the energy ω, and ε shows the energy-dependence of the two-cluster RGM kernel $V + \varepsilon K$ in the Pauli allowed space. In the present approach eliminating the energy dependence by introducing W, the $\widetilde{T}$-matrix does not have this energy dependence on ϵ [26]. By using $\widetilde{T}(\omega)$ in the Faddeev equations, one can eliminate the Pauli forbidden components in the relative motion of any pair of clusters. Care should be taken for a possible existence of trivial solutions of the Faddeev equation due to the relationship in Eq. (30).

The elimination of such redundant Faddeev components can easily be handled by introducing a subsidiary term, which is spelled out in Refs. [13,27] for the example of the 3α system.

Both methods give results agreeing within a few keV for the different systems considered here.

B. Microscopic models

In a microscopic description, the Hamiltonian of a A-body system is given by

$$H = \sum_{i=1}^{A} T_i - T_{\text{c.m.}} + \sum_{i>j=1}^{A} V_{ij}, \tag{31}$$

where T_i is the kinetic energy of nucleon i and V_{ij} an effective nucleon-nucleon interaction. Here also, two methods are available to derive three-cluster wave functions.

Let us first describe the microscopic three-cluster model based on the generator coordinate method [7]. The relative motions between the three clusters can be described by using two Jacobi coordinates between the cluster centers of mass. A variant of this model following the spirit of the hyperspherical method makes use of the hyper-radius and of the hypermomentum quantum number [28]. The microscopic wave functions read

$$\Psi^{JM\pi} = \sum_{\gamma K} \mathcal{A}\phi_1\phi_2\phi_3 \rho^{-5/2} \chi_{\gamma K}^{J\pi}(\rho) \mathcal{Y}_{\gamma K}^{JM}(\Omega_5), \tag{32}$$

where ρ and Ω_5 now refer to the relative motion of the centers of mass of the clusters.

Let $\boldsymbol{R}_1$ and $\boldsymbol{R}_2$ be two generator coordinates corresponding to the Jacobi coordinates $\boldsymbol{x}_1, \boldsymbol{x}_2$. They can be replaced by a generator coordinate R associated with the hyper-radius and five hyperangular generator coordinates Ω_{5R} corresponding to the hyperangular variables Ω_5 in Eq. (32). Wave function $\Psi^{JM\pi}$ can be expressed as a combination of basis states

$$\Phi_{\gamma K}^{JM\pi}(R) = \int d\Omega_{5R} \mathcal{Y}_{\gamma K}^{JM}(\Omega_{5R})\, \Phi(\boldsymbol{R}_1, \boldsymbol{R}_2), \tag{33}$$

where $\Phi(\boldsymbol{R}_1, \boldsymbol{R}_2)$ is a linear combination of Slater determinants. The configuration space is thus spanned by a single generator coordinate R. The calculation of matrix elements is performed with three-center Slater determinants with $0s$ harmonic-oscillator states. Projection on the relative orbital momenta γ and on the hypermomentum K are then obtained by a numerical integration over the angles Ω_{5R} corresponding to the orientations of the Jacobi generator coordinates and over the generator hyperangle for fixed values of the generator hyper-radius. Practical calculations involve seven-dimensional numerical integrals. The obtained projected matrix elements calculated for different choices of the generator hyper-radius R allow a variational study of the system with a rather large basis involving up to thousand basis functions.

In the correlated-Gaussian expansion method [18,29,30], the wave function for the state in the microscopic model is assumed to be obtained in the form

$$\Psi_{\text{F}} = \sum_{i=1}^{\mathcal{K}} C_i \mathcal{A}\phi_1\phi_2\phi_3 G(A_i, \boldsymbol{x}). \tag{34}$$

The relative motion between the three clusters is described as the explicitly correlated Gaussian

$$G(A, \boldsymbol{x}) = \exp\left(-\frac{1}{2} \sum_{i,j=1}^{2} A_{ij} \boldsymbol{x}_i \cdot \boldsymbol{x}_j \right) \tag{35}$$

containing three variational parameters $A_{11}, A_{12}(=A_{21}), A_{22}$ which are the elements of the 2×2 matrix A. Here $\boldsymbol{x}$ stands for appropriate Jacobi coordinates $\boldsymbol{x}_1, \boldsymbol{x}_2$. The overlap and Hamiltonian matrix elements are evaluated with the aid of an integral transformation which relates the correlated Gaussian to a product of single-particle Gaussian wave packets with equal width parameter. The latter representation makes it possible to calculate the matrix elements analytically (see Ref. [31] for detail). The trial wave function Ψ_{F} contains $3\mathcal{K}$ nonlinear parameters in matrices A_i as well as $\mathcal{K}$ linear parameters C_i. To determine A_i the optimization algorithm of the stochastic variational method [29,30] is efficiently used. The basis dimension of about $\mathcal{K} = 50$ is good enough to obtain converged solutions for both the 0_1^+ and 0_2^+ states of ^{12}C, as shown by Fig. 1 of Ref. [31].

V. RESULTS

A. Conditions of the calculations

We analyze three systems where a three-cluster structure is well established, i.e., ^{12}C, ^{9}Be, and ^{6}He. In each case, we perform a comparison of microscopic and semimicroscopic calculations with two effective forces: the Minnesota interaction (MN) [32] and the Volkov interaction V2 [33]. The Coulomb interaction is always included.

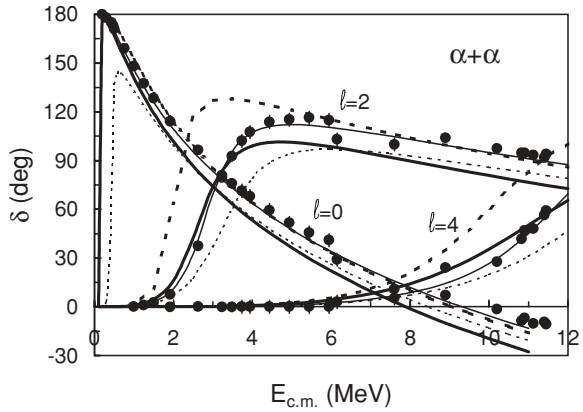

FIG. 3. $\alpha\alpha$ phase shifts. The solid lines are obtained with the standard potentials (a) and the dotted lines with $u = 0.9122$ and $M = 0.5820$ (thin curves: MN, thick curves: V2). The data are taken from Ref. [34].

For the microscopic description of ^{12}C, we have used the hyperspherical-harmonics method [28], and the stochastic variational method in a Gaussian basis [30]. For ^{9}Be and ^{6}He, only the hyperspherical-harmonics method has been used. The semimicroscopic results have been obtained, either with the Lagrange basis [15], or within the Faddeev approach [12]. When two methods are available, all displayed digits agree within both approaches.

For the physical constants, we use $\hbar^2/m_N = 41.472$ MeV fm^2 and the harmonic-oscillator parameter for the α cluster $b = 1.36$ fm ($\nu = 1/2b^2 = 0.270$ fm^{-2}). The $\alpha\alpha$ interaction is fitted on the phase shifts. We use $u = 0.94687$ for MN and $M = 0.605$ for V2 as standard values [14].

For the αn potential used in ^{6}He and ^{9}Be we adopt the MN interaction given in Ref. [15] ($u = 0.9474$), and the V2 force with the previous M value. A zero-range spin-orbit interaction is introduced, and is adjusted on the experimental $p3/2 - p1/2$ αn phase shifts. This gives $S_0 = 37$ MeV fm^5 for MN and $S_0 = 49$ MeV fm^5 for V2. The phase shifts are shown in Figs. 3 and 4 for $\alpha\alpha$ and αn, respectively. With the standard interaction, the agreement with experiment is quite good, as expected. As these interactions do not precisely reproduce the three-body binding energies, the interaction parameters will be slightly readjusted in the following. Typical values are illustrated in Figs. 3 and 4 as dotted lines. Even if the general trend is still valid, differences are significant, especially with the V2 force.

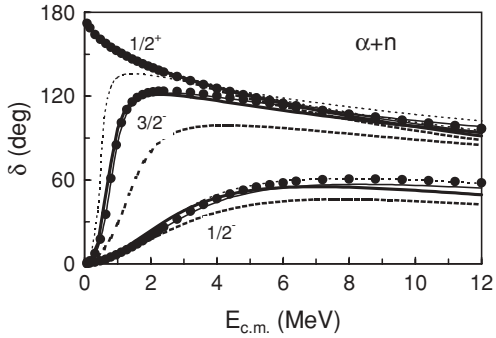

FIG. 4. αn phase shifts. The solid lines are obtained with the standard potentials (a) and the dotted lines with $u = 1.0045$ and $M = 0.6573$ (thin curves: MN, thick curves: V2). The data are taken from Ref. [35].

In the following we present rms radii and densities as tests of the wave functions. In all cases, the α radius and form factor are taken into account.

B. ^{12}C

We have already presented some results about ^{12}C in Ref. [19]. Here we make a more detailed comparison involving several potentials. The results are displayed in Table I.

First we discuss interaction (a) which reproduces the $\alpha\alpha$ phase shifts. While the MN interaction overbinds ^{12}C, the Volkov interaction V2 underbinds it. This confirms that a simultaneous description of the 2α and 3α systems is not possible with a high accuracy. The gaps between the microscopic and semimicroscopic models are rather similar (about 2.2 MeV) in spite of those differences. The 2^+ excitation energy is underestimated in all cluster calculations. This is a well-known drawback of the three-α model, where the spin-orbit force is absent.

In many cluster-model studies, the interaction is adjusted on the ground-state energy. This is necessary to provide a meaningful comparison of spectroscopic properties between different models. For example, the rms radius is known to be sensitive to the binding energy. We have used two different procedures: either we fit the interaction on the microscopic model (b) or on the semimicroscopic model (c). When the ground-state energies are fitted in case (b), the errors due to the

TABLE I. Comparison of ^{12}C energies (in MeV) from the 3α threshold and rms matter radii (in fm) with different potentials in the microscopic and semimicroscopic 3α models. Experimental energies are -7.27, 0.38, and -2.83 MeV for the 0_1^+, 0_2^+, and 2^+ states, respectively. In case (a), the forces reproduce $\alpha\alpha$ scattering while in cases (b)/(c) they reproduce the experimental 0_1^+ energy within the microscopic/semimicroscopic models.

J^π	Potential	Microscopic		Semimicroscopic	
		E	$\sqrt{\langle r^2\rangle}$	E	$\sqrt{\langle r^2\rangle}$
		(a)			
0_1^+	MN ($u = 0.94687$)	-11.61	2.18	-9.42	2.17
	V2 ($M = 0.605$)	-4.53	2.50	-2.33	2.68
0_2^+	MN ($u = 0.94687$)	0.71		0.52	
	V2 ($M = 0.605$)	1.64		1.23	
2^+	MN ($u = 0.94687$)	-9.22	2.16	-7.12	2.15
	V2 ($M = 0.605$)	-1.88	2.46	0.38	2.65
		(b)			
0_1^+	MN ($u = 0.9122$)	-7.27	2.25	-4.90	2.27
	V2 ($M = 0.5929$)	-7.27	2.41	-4.73	2.52
		(c)			
0_1^+	MN ($u = 0.93105$)	-9.57	2.21	-7.27	2.21
	V2 ($M = 0.5820$)	-9.99	2.35	-7.27	2.42

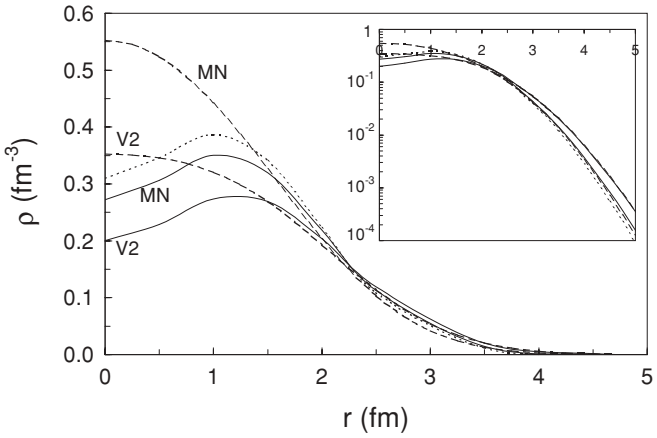

FIG. 5. Charge densities of ^{12}C with the MN and V2 potentials in the microscopic (solid lines) and semimicroscopic (dashed lines) models. The dotted line corresponds to the MN calculation (a). The inset represents the densities in a logarithmic scale.

semimicroscopic approximation become very similar. When the interaction is fitted on the ground-state energy, both models provide quite similar radii.

In Fig. 5, we present the monopole charge density $\rho(r)$ (denoted as $\rho_0(r)$ in Appendix B) for the ^{12}C ground state. In each case, the interaction reproduces the experimental binding energy [case (b) for the microscopic model, and case (c) for the semimicroscopic approximation]. The densities are normalized in such a way that

$$\int_0^\infty \rho(r) r^2 dr = Z/\sqrt{4\pi}, \tag{36}$$

with $Z = 6$. The microscopic densities are determined as explained in Ref. [36]. For the semimicroscopic approximation, we first determine the form factor, which is then converted to the density through a Fourier transform (some technical details are given in Appendix B).

Figure 5 confirms that the rms radii are larger with the V2 force than with the MN force. At small distances, the densities are lower with V2, and are therefore enhanced at large r values. Beyond 2 fm, the semimicroscopic model is a fair approximation. However, the short-distance behavior is different: whereas the microscopic approach provides a maximum near 1 fm and then decreases, the semimicroscopic density steadily increases when r tends to zero. This difference is probably due to three-body antisymmetrization effects, not included in the semimicroscopic approximation. To illustrate the sensitivity with respect to the binding energy, we also present the MN density in case (a), i.e., with an energy of -11.61 MeV (dotted line). The general trend is not affected, but the long-range part decreases more rapidly, which leads to an increase at short distances.

C. ^{9}Be

The results for ^{9}Be ($3/2^-$ ground state and $5/2^-$ first excited state) are displayed in Table II. We first consider in case (a) interactions agreeing with the phase shifts. With the MN interaction, the ^{9}Be ground state is overbound by about 1 MeV in the microscopic model. With V2 it is underbound by 0.2 MeV. As in ^{12}C, the semimicroscopic model provides smaller binding energies than the microscopic approach (0.45 MeV with MN and 0.24 MeV with V2). This means that three-body effects, missing in the semimicroscopic approximation, are expected to be attractive. With the MN potential, both models underbind the $5/2^-$ resonance, but the excitation energy is in all cases in fair agreement with experiment (2.42 MeV). For the $5/2^-$ resonance, the energies with V2 are positive, and should be considered as approximate values.

TABLE II. Comparison of ^{9}Be energies (in MeV) from the $\alpha\alpha n$ threshold and rms matter radii (in fm). Experimental energies are -1.57 and $+0.85$ MeV for the $3/2^-$, and $5/2^-$ states, respectively. See caption to Table I.

J^π	Potential	Microscopic		Semimicroscopic	
		E	$\sqrt{\langle r^2\rangle}$	E	$\sqrt{\langle r^2\rangle}$
		(a)			
$3/2^-$	MN ($u = 0.9474$)	-2.61	2.36	-2.16	2.41
	V2 ($M = 0.605$)	-1.36	2.60	-1.12	2.68
$5/2^-$	MN ($u = 0.9474$)	-0.09	2.39	0.2	
	V2 ($M = 0.605$)	≈ 1		≈ 1	
		(b)			
$3/2^-$	MN ($u = 0.9250$)	-1.57	2.43	-1.18	2.49
	V2 ($M = 0.6024$)	-1.57	2.58	-1.32	2.66
		(c)			
$3/2^-$	MN ($u = 0.9340$)	-1.97	2.40	-1.57	2.46
	V2 ($M = 0.5997$)	-1.81	2.56	-1.57	2.63

When the interactions are fitted to the experimental ground-state energies, the radii are close to each other. In Fig. 6, we present the neutron density $\rho(r)$ for the ^{9}Be ground state. In each case, the force parameters are taken to reproduce the experimental binding energy. Contrarily to ^{12}C, the microscopic calculation does not provide a hole in the density. Below 3 fm, the semimicroscopic model gives a rather uniform density, while the microscopic density is more peaked near the origin.

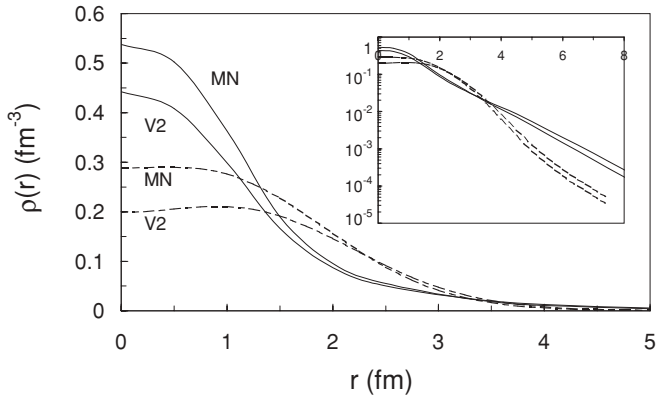

FIG. 6. Neutron densities of ^{9}Be with the MN and V2 potentials in the microscopic (solid lines) and semimicroscopic (dashed lines) models. The inset represents the densities in a logarithmic scale.

TABLE III. Comparison of ^{6}He energies (in MeV) from the $\alpha + 2n$ threshold and rms matter radii (in fm) obtained with different potentials in the microscopic and semimicroscopic αnn models. The experimental energy is -0.974 MeV See caption to Table I.

J^π	Potential	Microscopic		Semimicroscopic	
		E	$\sqrt{\langle r^2\rangle}$	E	$\sqrt{\langle r^2\rangle}$
		(a)			
0^+	MN ($u = 0.9474$)	-0.07	2.57	-0.08	2.93
	V2 ($M = 0.605$)	-2.43	2.46	-1.96	2.56
		(b)			
0^+	MN ($u = 1.0045$)	-0.98	2.38	-0.95	2.46
	V2 ($M = 0.6573$)	-0.98	2.90	-0.65	4.11
		(c)			
0^+	MN ($u = 1.0055$)	-1.02	2.37	-0.97	2.46
	V2 ($M = 0.6400$)	-1.43	2.74	-0.98	3.23

D. ^{6}He

^{6}He is the lightest nucleus considered here. Accordingly, three-body exchanges, missing in the semimicroscopic approximation, should play a minor role, and differences between both models should be reduced. This is confirmed by the results presented in Table III. Although ^{6}He is hardly bound with MN and overbound by about 1.5 MeV with V2, the differences between both models are small. In particular, the MN force provides virtually identical binding energies. The different qualitative properties of both forces appear very clearly for this weakly bound nucleus.

Let us turn to case (b) where both forces provide the same binding energy. The semimicroscopic model is again very accurate with MN and underestimates the energy by about 0.33 MeV with V2. Hence the accuracy of the semimicroscopic model depends more on the type of force than on the binding energy. The semimicroscopic approach provides an unrealistically large rms radius for ^{6}He.

In Fig. 7, we present the neutron density $\rho(r)$ for the ^{6}He ground state. In each case, the force parameters are taken

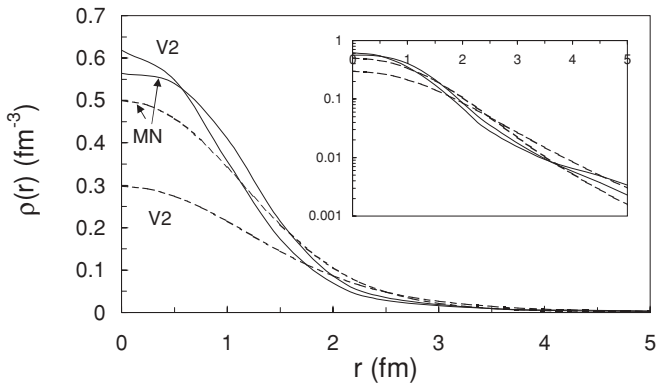

FIG. 7. Neutron densities of ^{6}He with the MN and V2 potentials in the microscopic (solid lines) and semimicroscopic (dashed lines) models. The inset represents the densities in a logarithmic scale.

TABLE IV. Comparison of the approximation $\lambda W^{(1)}$ with exact calculations involving W for the Minnesota interaction.

Nucleus	J^π	Exact W		$\lambda W^{(1)}$	
		E	$\sqrt{\langle r^2\rangle}$	E	$\sqrt{\langle r^2\rangle}$
^{12}C	0^+_1	-9.42	2.17	-9.83	2.19
^{9}Be	$3/2^-$	-2.16	2.41	-2.60	2.37
^{6}He	0^+	-0.95	2.46	-1.22	2.38

to reproduce the experimental binding energy. For the MN interaction, both approaches are very close to each other, in agreement with the rms radii. However, the behavior of the V2 result is somewhat different. The V2 force requires a rather strong readjustment of the admixture parameter to reproduce the ground-state energy. With the large M values of cases (b) and (c), the p-wave phase shifts are too repulsive (see Fig. 4). This is consistent with the unrealistic rms radius of Table III.

E. Validity of approximation $\lambda W^{(1)}$

The approximation proposed in Sec. III B is tested for the three systems in Table IV. One observes that its accuracy is quite good for $\alpha\alpha$, as shown by the ^{12}C results. It is much better than the intrinsic accuracy of the semimicroscopic model.

The approximation seems to be less valid for αn, since the error is larger for the other systems. In the ^{9}Be case, this error accidentally cancels the error due to the use of the semimicroscopic model. This is not true for ^{6}He, but a slight readjustment of the amplitude λ in the αN interaction would allow us to compensate the difference. Anyway, the approximation seems to be accurate enough for qualitative considerations.

VI. CONCLUSION

We analyze a new semimicroscopic model, with two-body interactions based on RGM kernels. The renormalized RGM potential provides the same phase shifts as the full RGM and is nonlocal, but energy independent. This allows us to avoid the problem of defining two-body energies in many-body calculations.

We have used this new interaction in a three-body model, and compared it with a fully microscopic approach. This is expected to evaluate the importance of antisymmetrization and three-body effects. The model has been applied to ^{6}He, ^{9}Be, and ^{12}C, and the importance of the nucleon-nucleon interaction has been tested by using two forces (MN and V2). The mixture parameters involved in these forces have been determined on the $\alpha\alpha$ and αn phase shifts.

The use of effective interactions is necessary in cluster theories. Introducing realistic forces would require to go beyond the cluster approximation, i.e., to use *ab initio* models [4]. These models are well adapted to the spectroscopy of light nuclei (currently up to about $A \approx 12$). However their extension to resonances and continuum states is still very difficult. In particular the relative simplicity of the cluster model will

remain useful in reaction models, or for the description of three-body continuum states.

Our work shows that neither the microscopic model nor its approximation are able to precisely reproduce two-cluster and three-cluster properties simultaneously. In general the differences between both approaches are small, and decrease with the nucleon number (2.5 MeV for ^{12}C, 0.5 MeV for ^{9}Be and ^{6}He). For ^{12}C, the renormalized RGM provides a good description of low-lying states. This represents a significant improvement with respect to previous nonmicroscopic works, where ambiguities appear [15]. The differences between the fully microscopic and semimicroscopic approaches depend on the NN force; they are smaller for MN than for V2. The V2 force presents some peculiarities. It is known to overestimate clustering effects. The semimicroscopic approach provides an unrealistically large rms radius for ^{6}He. This confirms that the V2 force is probably not well adapted to light systems.

With the densities, the differences between both models are more apparent than with the rms matter radii. In general, differences occur at short distances or, in other words, at large momenta in the form factors. In the simplest nucleus ^{6}He with the MN interaction, the densities derived from the microscopic model and from its approximation are very similar to each other.

In all cases the binding energies are slightly *underestimated* by the semimicroscopic approach. This means that three-body effects, missing in this approximation, should be *attractive*. The derivation of reliable three-cluster forces is a challenge for future works.

ACKNOWLEDGMENTS

This text presents research results of Bilateral Joint Research Projects of JSPS (2006–2008), Grants-in-Aid for Scientific Research from JSPS (No. 18540261), a Grant for Promotion of Niigata University Research Projects (2005–2007), the FRFC (Belgium) contract No. 2.4604.07, and the IAP program P6/23 initiated by the Belgian-state Federal Services for Scientific, Technical and Cultural Affairs. M.T. acknowledges a financial support of IISN, Belgium. P.D. acknowledges the support of FNRS, Belgium.

APPENDIX A: MATRIX ELEMENTS OF NONLOCAL KERNELS IN HARMONIC-OSCILLATOR BASIS

When the NN potential has a Gaussian radial form, the nonlocal integral kernels $\mathcal{O}(\boldsymbol{r}, \boldsymbol{r}')$ which appear in $\alpha + N$ and $\alpha + \alpha$ have the following form:

$$\mathcal{O} = \mathrm{e}^{-\frac{1}{2}\tilde{\boldsymbol{x}}A\boldsymbol{x}}, \quad \tilde{\boldsymbol{x}}Q\boldsymbol{x}\mathrm{e}^{-\frac{1}{2}\tilde{\boldsymbol{x}}A\boldsymbol{x}}, \quad f(|\tilde{\omega}\boldsymbol{x}|)\mathrm{e}^{-\frac{1}{2}\tilde{\boldsymbol{x}}A\boldsymbol{x}}. \tag{A1}$$

Here we use the matrix notations to simplify expressions: $\boldsymbol{x}$ is now a 2×1 matrix whose elements are $\boldsymbol{r}$ and $\boldsymbol{r}'$ (note that $\boldsymbol{x}$ and A used in Sec. IV have a different meaning from that defined here), $\tilde{\boldsymbol{x}}$ its transpose, A and Q are 2×2 symmetric matrices, and ω is a 2×1 matrix. The function $f(s)$ is either $1/s$ or $\mathrm{erf}(\mu s)/s$ as it comes from the Coulomb potential.

To obtain the matrix element

$$\langle \psi_{n\ell m} | \mathcal{O} | \psi_{n'\ell'm'} \rangle, \tag{A2}$$

we make use of the generating function of the harmonic-oscillator functions [30,37]

$$\begin{aligned} A(\boldsymbol{k}, \boldsymbol{r}) &= \left(\frac{\nu}{\pi}\right)^{3/4} \exp\left(-\frac{1}{2}\boldsymbol{k}^2 + \sqrt{2\nu}\boldsymbol{k}\cdot\boldsymbol{r} - \frac{1}{2}\nu\boldsymbol{r}^2\right) \\ &= \sum_{n\ell m} \psi^*_{n\ell m}(\boldsymbol{r}) P_{n\ell m}(\boldsymbol{k}), \end{aligned} \tag{A3}$$

where ν is the oscillator constant and

$$P_{n\ell m}(\boldsymbol{k}) = \sqrt{\frac{B_{n\ell}}{(2n+\ell)!}} k^{2n+\ell} Y_{\ell m}(\Omega_k) \tag{A4}$$

is the Bargmann transform of the HO wave function in a spherical basis with

$$B_{n\ell} = \frac{4\pi(2n+\ell)!}{2^n n!(2n+2\ell+1)!!}. \tag{A5}$$

Let us consider the quantity

$$\mathcal{I} = \iint A(\boldsymbol{k}, \boldsymbol{r}) \mathcal{O}(\boldsymbol{r}, \boldsymbol{r}') A(\boldsymbol{k}', \boldsymbol{r}') d\boldsymbol{r}\, d\boldsymbol{r}'. \tag{A6}$$

Inserting the expansion (A3) in the above equation we obtain

$$\mathcal{I} = \sum_{n\ell m} \sum_{n'\ell'm'} \langle \psi_{n\ell m} | \mathcal{O} | \psi_{n'\ell'm'} \rangle P_{n\ell m}(\boldsymbol{k}) P^*_{n'\ell'm'}(\boldsymbol{k}'). \tag{A7}$$

Thus the calculation of the matrix element proceeds as follows. First we calculate $\mathcal{I}$ and then expand it in power series of $\boldsymbol{k}$ and $\boldsymbol{k}'$. By comparing the expansion with Eq. (A7), we get the needed matrix element (A2).

As an illustration we carry out two cases. The first is for $\mathcal{O} = \mathrm{e}^{-\frac{1}{2}\tilde{\boldsymbol{x}}A\boldsymbol{x}}$. Then we obtain

$$\mathcal{I} = \left(\frac{4\pi\nu}{\det(A+C)}\right)^{3/2} \mathrm{e}^{pk^2 + p'k'^2 + q\boldsymbol{k}\cdot\boldsymbol{k}'}, \tag{A8}$$

where C is a 2×2 matrix with $C_{ij} = \nu\delta_{i,j}$, and

$$\begin{aligned} p &= -\tfrac{1}{2} + \nu\{(A+C)^{-1}\}_{11}, \\ p' &= -\tfrac{1}{2} + \nu\{(A+C)^{-1}\}_{22}, \\ q &= 2\nu\{(A+C)^{-1}\}_{12}. \end{aligned} \tag{A9}$$

It is easy to obtain the following result:

$$\begin{aligned} &\langle \psi_{n\ell m} | \mathrm{e}^{-\frac{1}{2}\tilde{\boldsymbol{x}}A\boldsymbol{x}} | \psi_{n'\ell'm'} \rangle \\ &= \delta_{\ell,\ell'}\delta_{m,m'} \left(\frac{4\pi\nu}{\det(A+C)}\right)^{3/2} \sqrt{\frac{(2n+\ell)!(2n'+\ell)!}{B_{n\ell}B_{n'\ell}}} \\ &\quad \times \sum_k B_{k\ell} \frac{p^{n-k} p'^{n'-k} q^{2k+\ell}}{(n-k)!(n'-k)!(2k+\ell)}. \end{aligned} \tag{A10}$$

The sum extends to $k = 0, 1, \ldots, \min(n, n')$.

Next we consider the Coulomb potential with $f(s) = 1/s$. The corresponding integral is obtained in a form

$$\begin{aligned} \mathcal{I} = &\left(\frac{4\pi\nu}{\det(A+C)}\right)^{3/2} \sqrt{\frac{2\gamma}{\pi}} \mathrm{e}^{pk^2 + p'k'^2 + q\boldsymbol{k}\cdot\boldsymbol{k}'} \\ &\times M(\sqrt{\gamma\nu}|\rho_1\boldsymbol{k} + \rho_2\boldsymbol{k}'|), \end{aligned} \tag{A11}$$

where

$$\rho_1 = (\widetilde{\omega}(A+C)^{-1})_1, \quad \rho_2 = (\widetilde{\omega}(A+C)^{-1})_2,$$
$$\gamma = (\rho_1\omega_1 + \rho_2\omega_2)^{-1} = (\widetilde{\omega}(A+C)^{-1}\omega)^{-1}, \tag{A12}$$

and

$$M(z) = \int_0^1 \mathrm{e}^{-z^2t^2}dt = \frac{\sqrt{\pi}}{2}\frac{1}{z}\mathrm{erf}z. \tag{A13}$$

The required matrix element is given as follows:

$$\begin{aligned}
&\langle\psi_{n\ell m}|\frac{1}{|\widetilde{\omega}\boldsymbol{x}|}\mathrm{e}^{-\frac{1}{2}\widetilde{\boldsymbol{x}}A\boldsymbol{x}}|\psi_{n'\ell'm'}\rangle \\
&= \delta_{\ell,\ell'}\delta_{m,m'}\left(\frac{4\pi\nu}{\det(A+C)}\right)^{3/2}\sqrt{\frac{2\gamma}{\pi}}\sqrt{\frac{(2n+\ell)!(2n'+\ell)!}{B_{n\ell}B_{n'\ell}}} \\
&\quad\times\sum_k B_{k\ell}\frac{1}{(n-k)!(n'-k)!(2k+\ell)!} \\
&\quad\times\int_0^1 {p_1}^{n-k}{p_2}^{n'-k}{p_{12}}^{2k+\ell}dt,
\end{aligned} \tag{A14}$$

where

$$p_1 = p - \gamma\nu\rho_1^2t^2, \quad p_2 = p' - \gamma\nu\rho_2^2t^2,$$
$$p_{12} = q - 2\gamma\nu\rho_1\rho_2t^2. \tag{A15}$$

The matrix element of the folded Coulomb potential $\langle\psi_{n\ell m}|\frac{1}{|\widetilde{\omega}\boldsymbol{x}|}\mathrm{erf}\,(\mu|\widetilde{\omega}\boldsymbol{x}|)\mathrm{e}^{-\frac{1}{2}\widetilde{\boldsymbol{x}}A\boldsymbol{x}}|\psi_{n'\ell'm'}\rangle$ can simply be obtained by replacing γ in Eqs. (A14) and (A15) with $2\mu^2\gamma/(2\mu^2+\gamma)$.

APPENDIX B: FORM FACTORS AND DENSITIES

In a microscopic model, the charge density and form factor operators are defined as

$$\hat{\rho}(\boldsymbol{r}) = \sum_i^A\left(\frac{1}{2} - t_{iz}\right)\delta(\boldsymbol{r}_i - \boldsymbol{R}_{\mathrm{c.m.}} - \boldsymbol{r}),$$
$$\hat{F}(\boldsymbol{q}) = \frac{1}{Z}\sum_i^A\left(\frac{1}{2} - t_{iz}\right)\exp[i\boldsymbol{q}\cdot(\boldsymbol{r}_i - \boldsymbol{R}_{\mathrm{c.m.}})], \tag{B1}$$

where t_{iz}, $\boldsymbol{r}_i$ and $\boldsymbol{R}_{\mathrm{c.m.}}$ are the isospin z-component and coordinate of nucleon i, and the c.m. coordinate of the system, respectively. The neutron density and form factor operators are obtained in a similar way. The matter density is just the sum of the proton and neutron densities. Here and in the following, we use the notation $\hat{O}$ for an operator, and O for its matrix elements. The charge density and the form factor are related to each other through

$$\rho(\boldsymbol{r}) = \frac{Z}{(2\pi)^3}\int\exp(i\boldsymbol{q}\cdot\boldsymbol{r})F(\boldsymbol{q})d\boldsymbol{q}. \tag{B2}$$

They are determined as explained in Ref. [36]. Owing to the Gaussian orbitals used in the Generator Coordinate Method, the densities can be easily computed, and the Fourier transform (B2) is not necessary.

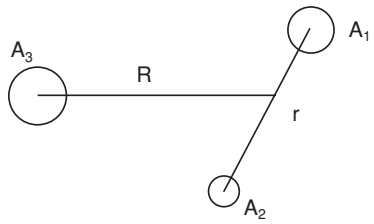

FIG. 8. Coordinate system in the three-cluster model.

The density and the form factor are usually expanded in multipoles as

$$\rho(\boldsymbol{r}) = \sum_\lambda \rho_\lambda(r)Y_{\lambda0}(\Omega_r),$$
$$F(\boldsymbol{q}) = \sum_\lambda F_\lambda(q)Y_{\lambda0}(\Omega_q), \tag{B3}$$

where $\rho_\lambda(r)$ and $F_\lambda(r)$ are the multipolar densities and form factors, respectively. For zero spin nuclei, such as ^{6}He or ^{12}C, the density is spherically symmetric ($\lambda = 0$ only). The relationship between $\rho_\lambda(r)$ and $F_\lambda(r)$ is obtained with Eq. (B2) as

$$\rho_\lambda(r) = \frac{Z}{2\pi^2}i^\lambda\int j_\lambda(qr)F_\lambda(q)q^2dq. \tag{B4}$$

In a nonmicroscopic cluster model, the form factor operator is defined as

$$\hat{F}(\boldsymbol{q}) = \frac{1}{Z}\sum_{j=1}^N Z_jF_j(\boldsymbol{q})\exp[i\boldsymbol{q}\cdot(\boldsymbol{r}_j - \boldsymbol{R}_{\mathrm{c.m.}})], \tag{B5}$$

where N is the number of clusters, and Z_j and $F_j(\boldsymbol{q})$ are the charge and form factor of cluster j. Equation (B2) is still valid to determine the associated density. In order to be consistent with the microscopic approach, the internal form factors are defined in the HO shell model. For s-shell nuclei, the form factor is given by

$$F_j(\boldsymbol{q}) = \exp\left[-q^2b^2\frac{(A_j-1)}{4A_j}\right], \tag{B6}$$

where A_j is the nucleon number of cluster j.

In the three-cluster model the form factor operator (B3) is written as

$$\begin{aligned}
\hat{F}(\boldsymbol{q}) = \frac{1}{Z}\Bigg[&Z_1F_1(\boldsymbol{q})\exp\left(i\boldsymbol{q}\cdot\left(\frac{A_3}{A}\boldsymbol{R} + \frac{A_2}{A_{12}}\boldsymbol{r}\right)\right) \\
&+ Z_2F_2(\boldsymbol{q})\exp\left(i\boldsymbol{q}\cdot\left(\frac{A_3}{A}\boldsymbol{R} - \frac{A_1}{A_{12}}\boldsymbol{r}\right)\right) \\
&+ Z_3F_3(\boldsymbol{q})\exp\left(-i\frac{A_{12}}{A}\boldsymbol{q}\cdot\boldsymbol{R}\right)\Bigg],
\end{aligned} \tag{B7}$$

where we have used the coordinate system of Fig. 8 ($A_{12} = A_1 + A_2$). Each term is expanded in multipoles with the help of

$$\exp(i\boldsymbol{q}\cdot\boldsymbol{r})$$
$$= 4\pi\sum_{\lambda\mu}i^\lambda j_\lambda(qr)Y^\star_{\lambda\mu}(\Omega_q)Y_{\lambda\mu}(\Omega_r),$$

$$j_\lambda(|\alpha \boldsymbol{R} + \beta \boldsymbol{r}|) Y_{\lambda\mu}(\Omega_{\alpha \boldsymbol{R}+\beta \boldsymbol{r}}) = \sum_{\ell_1,\ell_2} i^{\ell_1+\ell_2-\lambda} [4\pi(2\ell_1+1)(2\ell_2+1)/(2\lambda+1)]^{1/2} \times \langle \ell_1 \ell_2 00|\lambda 0\rangle\, j_{\ell_1}(\alpha R) j_{\ell_2}(\beta r) \big[Y_{\ell_1}(\Omega_R) \otimes Y_{\ell_2}(\Omega_r)\big]_{\lambda\mu}. \tag{B8}$$

This provides us with the multipolar form factor. In particular, the monopole term reads

$$\frac{Z}{\sqrt{4\pi}} \hat{F}_0(q) = Z_3 F_3(\boldsymbol{q}) j_0\left(\frac{A_{12}}{A} q R\right) + 4\pi \sum_L (2L+1)^{1/2} \times [Y_L(\Omega_R) \otimes Y_L(\Omega_r)]_{00}\, j_L\left(\frac{A_3}{A} q R\right) \times \left[Z_1 F_1(\boldsymbol{q}) j_L\left(\frac{A_2}{A_{12}} q r\right) + (-1)^L Z_2 F_2(\boldsymbol{q}) j_L\left(\frac{A_1}{A_{12}} q r\right)\right]. \tag{B9}$$

Finally, we have to determine the matrix elements of this operator between basis functions (26), (27). First, coordinates R and r are expressed as a function of ρ and α. The integration over (Ω_R, Ω_r) is performed analytically; for the hyperangle α, we use a Fourier quadrature. Owing to the use of Lagrange functions combined with the Gauss approximation, the integration over the hyper-radius reduces to a simple evaluation of Bessel functions at the mesh points. The multipolar densities are determined from (B4) through a numerical integration over momentum q. In practice, values up to $q \sim 10$ fm^{-1} are involved to get a good precision on the densities at short distances. The summation over L in (B9) is carried out up to $L \sim 6$–8.

[1] K. Wildermuth and Y. C. Tang, *A Unified Theory of the Nucleus* (Vieweg, Braunschweig, 1977).
[2] S. Saito, Prog. Theor. Phys. Suppl. **62**, 11 (1977).
[3] Y. C. Tang, in *Topics in Nuclear Physics II*, Lecture Notes in Physics (Springer, Berlin, 1981), Vol. 145, p. 572.
[4] S. C. Pieper, R. B. Wiringa, and J. Carlson, Phys. Rev. C **70**, 054325 (2004).
[5] M. Kamimura, Nucl. Phys. **A351**, 456 (1981).
[6] E. Uegaki, Y. Abe, S. Okabe, and H. Tanaka, Prog. Theor. Phys. **62**, 1621 (1979).
[7] P. Descouvemont and D. Baye, Phys. Rev. C **36**, 54 (1987).
[8] J. L. Visschers and R. Van Wageningen, Phys. Lett. **B34**, 455 (1971).
[9] Yu. F. Smirnov, I. T. Obukhovsky, Yu. M. Tchuvil'sky, and V. G. Neudatchin, Nucl. Phys. **A235**, 289 (1974).
[10] E. M. Tursunov, J. Phys. G **27**, 1381 (2001).
[11] E. M. Tursunov, D. Baye, and P. Descouvemont, Nucl. Phys. **A723**, 365 (2003).
[12] Y. Fujiwara, H. Nemura, Y. Suzuki, K. Miyagawa, and M. Kohno, Prog. Theor. Phys. **107**, 745 (2002).
[13] Y. Fujiwara, Y. Suzuki, K. Miyagawa, M. Kohno, and H. Nemura, Prog. Theor. Phys. **107**, 993 (2002).
[14] Y. Fujiwara, K. Miyagawa, M. Kohno, Y. Suzuki, D. Baye, and J.-M. Sparenberg, Phys. Rev. C **70**, 024002 (2004).
[15] M. Theeten, D. Baye, and P. Descouvemont, Phys. Rev. C **74**, 044304 (2006).
[16] W. Timm, H. R. Fiebig, and H. Friedrich, Phys. Rev. C **25**, 79 (1982).
[17] E. W. Schmid, Nucl. Phys. **A416**, 347c (1984).
[18] Y. Suzuki, R. G. Lovas, K. Yabana, and K. Varga, *Structure and Reactions of Light Exotic Nuclei* (Taylor & Francis, London, 2003).
[19] Y. Suzuki, H. Matsumura, M. Orabi, Y. Fujiwara, P. Descouvemont, M. Theeten, and D. Baye, Phys. Lett. B (in press).
[20] H. Horiuchi, Prog. Theor. Phys. Suppl. **62**, 90 (1977).
[21] B. Buck, H. Friedrich, and C. Wheatley, Nucl. Phys. **A275**, 246 (1977).
[22] S. Ali and A. R. Bodmer, Nucl. Phys. **80**, 99 (1966).
[23] P. Descouvemont, C. Daniel, and D. Baye, Phys. Rev. C **67**, 044309 (2003).
[24] M. Theeten, D. Baye, and P. Descouvemont, Nucl. Phys. **A753**, 233 (2005).
[25] D. Baye and P.-H. Heenen, J. Phys. A **19**, 2041 (1986).
[26] Y. Fujiwara, M. Kohno, and Y. Suzuki, Few-Body Syst. **34**, 237 (2004).
[27] Y. Fujiwara, Y. Suzuki, and M. Kohno, Phys. Rev. C **69**, 037002 (2004).
[28] S. Korennov and P. Descouvemont, Nucl. Phys. **A740**, 249 (2004).
[29] K. Varga and Y. Suzuki, Phys. Rev. C **52**, 2885 (1995).
[30] Y. Suzuki and K. Varga, *Stochastic Variational Approach to Quantum-Mechanical Few-Body Problems*, Lecture Notes in Physics, Vol. m54 (Springer, Berlin, 1998).
[31] H. Matsumura and Y. Suzuki, Nucl. Phys. **A739**, 238 (2004).
[32] D. R. Thompson, M. LeMere, and Y. C. Tang, Nucl. Phys. **A286**, 53 (1977).
[33] A. B. Volkov, Nucl. Phys. **74**, 33 (1965).
[34] S. A. Afzal, A. Ahmed, and S. Ali, Rev. Mod. Phys. **41**, 247 (1969).
[35] G. L. Morgan and R. L. Walter, Phys. Rev. **168**, 1114 (1968).
[36] D. Baye, P. Descouvemont, and N. K. Timofeyuk, Nucl. Phys. **A577**, 624 (1994).
[37] K. T. Hecht and Y. Suzuki, J. Math. Phys. **24**, 785 (1983).